THE JOURNAL OF PHYSICAL CHEMISTRY Letters

Perspective

pubs.acs.org/JPCL

Infrared Chemical Nano-Imaging: Accessing Structure, Coupling, and Dynamics on Molecular Length Scales

Eric A. Muller, Benjamin Pollard, and Markus B. Raschke*

Department of Physics, Department of Chemistry, and JILA, University of Colorado, Boulder, Colorado 80309, United States

ABSTRACT: This Perspective highlights recent advances in infrared vibrational chemical nano-imaging. In its implementations of scattering scanning near-field optical microscopy (*s*-SNOM) and photothermal-induced resonance (PTIR), IR nanospectroscopy provides few-nanometer spatial resolution for the investigation of polymer, biomaterial, and related soft-matter surfaces and nanostructures. Broad-band IR *s*-SNOM with coherent laser and synchrotron sources allows for chemical recognition with small-ensemble sensitivity and the potential for sensitivity reaching the single-molecule limit. Probing selected vibrational marker resonances, it gives access to nanoscale chemical imaging of composition, domain morphologies, order/disorder, molecular orientation, or crystallographic phases. Local intra- and intermolecular coupling can be measured through frequency shifts of a vibrational marker in heterogeneous environments and associated inhomogeneities in vibrational dephasing. In combination with ultrafast spectroscopy, the vibrational coherent evolution of homogeneous sub-ensembles coupled to their environment can be observed. Outstanding challenges are discussed in terms of extensions to coherent and multidimensional spectroscopies, implementation in liquid and in situ environments, general sample limitations, and engineering *s*-SNOM scanning probes to better control the nano-localized optical excitation and to increase sensitivity.

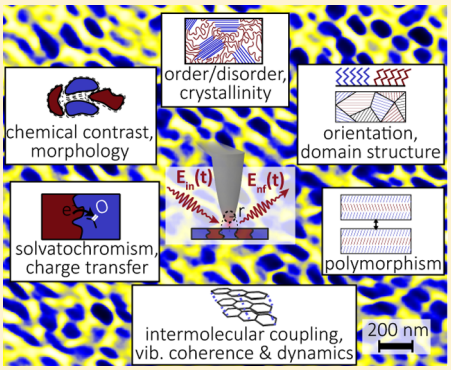

Optical Nano-Imaging of Molecular Matter. Heterogeneity underlies many properties of functional materials. The spatial distribution of different chemical constituents and the resulting complex interrelationship between structure, coupling, and dynamics define the macroscopic response of these materials. Properties ranging from structural performance to charge carrier mobility and dynamics are determined by the identity and distribution of constituent molecules, polymorphism, grain size and packing, internal boundaries, and defects. The length scales of the associated microscopic processes that control, for example, the performance of catalytic, biological, or photophysical systems are typically on the mesoscale of tens of nanometers to micrometers.

Chemical imaging with the desired spatial resolution is possible with X-ray and electron microscopy, through element- and bonding-specific spectroscopies[1] with the ultrahigh spatial resolution provided by their short wavelengths.[2] In optical microscopy, nanometer spatially resolved imaging even in the optical far-field can be achieved using fluorescent emitters as local probes, allowing for *in situ* imaging of biological structures.[3,4]

Near-field microscopy offers, in principle, the most generalized approach to beyond diffraction-limited optical imaging.[5−8] The spatially confined optical near-field light−matter interaction provides intrinsic diffraction-unlimited spatial resolution. Near-field microscopy can, in general, be implemented with any optical process and at essentially any wavelength from the ultraviolet to THz. With notable recent advances in linear, nonlinear, coherent, and ultrafast near-field spectroscopy and imaging, electronic and structural parameters

The spatially confined optical near-field light−matter interaction provides intrinsic diffraction-unlimited spatial resolution.

are now accessible, including coupling and dynamics in materials down to the atomic and molecular scale.

Instead of a comprehensive review, we focus on recent developments, outstanding challenges, and fundamental limitations of chemical infrared (IR) nano-imaging of molecular and soft-matter to provide ultrahigh spatial, spectral, and temporal resolution with exquisite sensitivity and specificity. IR nano-imaging complements related advances in tip-enhanced Raman scattering (TERS), yet is generally more versatile for soft-matter applications with favorable IR selection rules for the primary vibrational modes of interest.

IR nanospectroscopy offers simultaneous spectroscopic access to the relationship of chemical identity and morphology of molecular matter with molecular-level spectroscopic specificity and spatial resolution, as illustrated in Figure 1. The sensitivity to bond orientation and packing can be used to measure disorder, structural orientation, and polymorphism. Through spectral changes due to vibronic coupling and vibrational solvatochromism, we show how the technique

Received: January 19, 2015
Accepted: March 18, 2015

DOI: 10.1021/acs.jpclett.5b00108
J. Phys. Chem. Lett. 2015, 6, 1275−1284

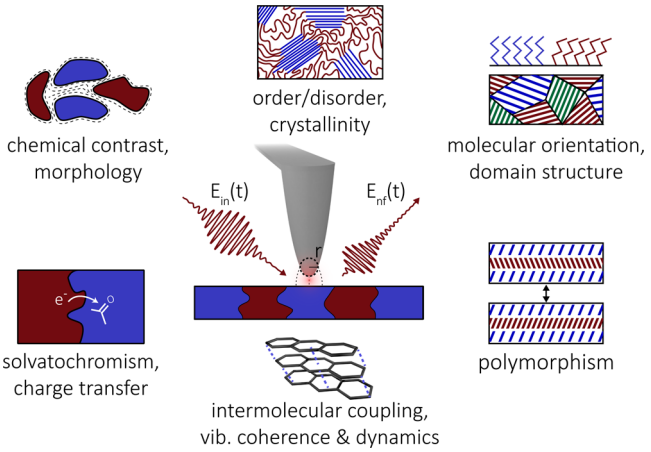

Figure 1. Chemical composition and structure, with associated coupling and dynamics, define the properties and function in heterogeneous functional materials. IR *s*-SNOM vibrational nano-spectroscopy allows imaging of chemical composition, anisotropy, order, or crystallinity through polarization selectivity, spectral position, and line width. It can furthermore distinguish between different polymorphs and probe charge transfer and intermolecular coupling through vibrational solvatochromism or ultrafast coherent and structural dynamics.

gives insight into coupled electronic structure, local electric fields, and charge transfer. In its ultrafast dynamic implementation, we discuss how coherent energy transfer and competing relaxation pathways can be resolved on femtosecond time scales, with a perspective on multidimensional nano-imaging. We discuss experimental challenges associated in terms of IR generation, access to *in situ* and liquid environments, and in pushing the sensitivity frontier toward single-molecule spectroscopy. We also cover sample constraints and limits of the technique as a surface probe.

IR Nano-Imaging and -Spectroscopy. The combination of IR vibrational spectroscopy with advanced scanning probe microscopies provides for wavelength-independent super-resolution IR microscopy in different modalities. The two primary IR nanoprobe modalities are scattering scanning near-field microscopy (*s*-SNOM)[5,7,9−11] and photothermal-induced resonance (PTIR)[12] imaging, representing optical and mechanical detection, respectively. We begin with a brief summary of the imaging contrast mechanism, signal detection, and general light source requirements. For details, the reader is referred to the technical literature and in-depth reviews.[13,14]

In *s*-SNOM, IR light is focused on the apex of a sharp metallic AFM tip. The high spatial frequencies (**k**-vectors) provided by the near-field of the tip apex localize the optical light−matter interaction to dimensions given by the apex radius $r \propto 1/k$, to first order defining the spatial resolution. The signal of interest arises from the mutual near-field tip−sample optical polarization, resonantly enhanced as the incident IR wavelength matches vibrational modes in the sample. By scanning across the sample while detecting the tip-scattered light, the optical response of the sample is mapped with nanometer spatial resolution.

Near-Field Signal Detection. Many initial technical difficulties in detecting the spatially localized near-field signal and separating it from the unspecific far-field background have been overcome in recent years, through tip−sample distance modulation in combination with different homodyne[15−18] and heterodyne[19,20] amplification techniques. The cantilever that supports the tip is dithered by a few 10s of nm, as is also the routine basis of the simultaneously recorded noncontact atomic force microscope (AFM) image. By demodulating the signal from a single-pixel optical detector at higher harmonics of the motion of the tip ($2\omega_{tip}$, $3\omega_{tip}$, ...) using lock-in amplification, the contribution from just the nonlinear variation of the near-field interaction can be isolated with increasing near- to far-field contrast, albeit at the expense of signal strength.[21]

The complex valued near-field signal $\tilde{E}_{nf}$ of interest is given by $\tilde{E}_{nf}(\bar{\nu}) = \mathrm{Re}\{\tilde{E}_{nf}(\bar{\nu})\} + \mathrm{Im}\{\tilde{E}_{nf}(\bar{\nu})\} = |A|_{nf}(\bar{\nu})e^{i\phi_{nf}(\bar{\nu})}$. This weak tip-scattered field interferes with a far-field background scattered by the tip and sample, leading to a self-homodyne amplified signal with uncontrolled phase.[22] A reference field is therefore typically applied as part of an asymmetric Michelson interferometer (Figure 2a) to actively control the reference phase for homo- or heterodyne detection. Primarily three optical fields contribute to the total detector signal:[23] tip-mediated near-field scattered radiation $\tilde{E}_{nf}$, far-field background $\tilde{E}_{bg}$, and the reference field $\tilde{E}_{ref}$. The resulting detected intensity I, with leading order terms after lock-in detection at higher-

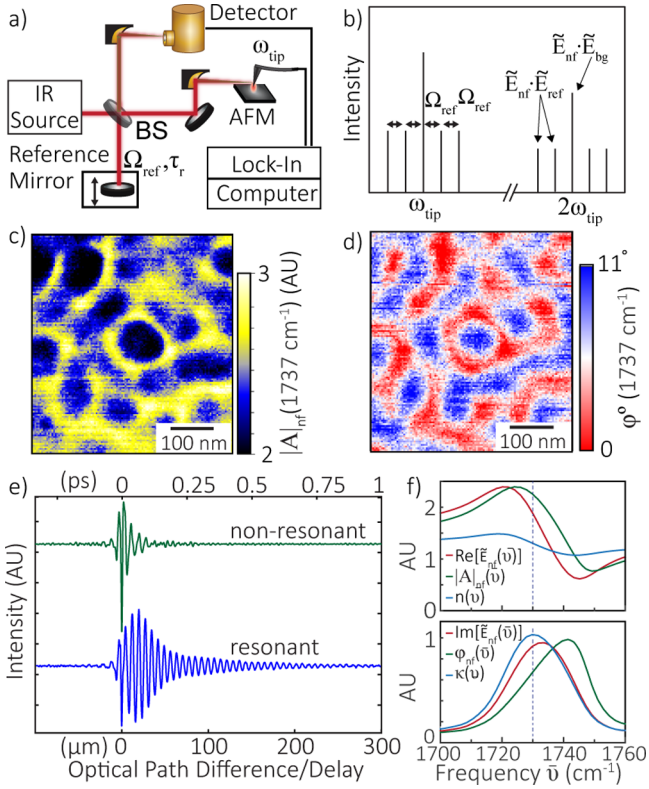

Figure 2. (a) Schematic of *s*-SNOM with interferometric detection. (b) Frequency spectrum of the *s*-SNOM signal at harmonics of the tip dither frequency ω_{tip}. Sidebands created by reference field modulation Ω_{ref} separate the phase-reference signal $\tilde{E}_{nf}\tilde{E}_{ref}\cos(\phi_{nf})$ from the self-homodyne signal $\tilde{E}_{nf}\tilde{E}_{bg}\cos(\phi_{bg})$. (c,d) Example of chemical *s*-SNOM amplitude $|A|_{nf}(\bar{\nu})$ (c) and phase $\phi_{nf}(\bar{\nu})$ (d) maps of the carbonyl resonance in a block copolymer. (e) *s*-SNOM asymmetric interferogram using a broad-band IR source. (f) *s*-SNOM spectral shifts relative to spectral ellipsometry calculated by the spherical dipole model for a strong molecular oscillator. The index of refraction $n(\bar{\nu})$ and extinction coefficient $\kappa(\bar{\nu})$ of poly(methyl methacrylate) (PMMA) from spectral ellipsometry show the carbonyl stretch at 1730 cm^{-1}. The calculated $\mathrm{Im}\{\tilde{E}_{nf}(\bar{\nu})\}$ (red) is shifted by 4 cm^{-1}, and $\phi_{nf}(\bar{\nu})$ (green) is shifted by 11 cm^{-1} compared to $\kappa(\bar{\nu})$ (blue).

DOI: 10.1021/acs.jpclett.5b00108
J. Phys. Chem. Lett. 2015, 6, 1275−1284

order harmonics of the tip frequency ω_{tip}, is given by $I \propto \tilde{E}_{nf}\tilde{E}_{bg}\cos(\phi_{nf} - \phi_{bg}) + \tilde{E}_{nf}\tilde{E}_{ref}\cos(\phi_{nf} - \phi_{ref})$.

Different interferometric detection schemes, both for spectrally narrow as well as broad-band *s*-SNOM, have been developed. All of these methods aim to extract the near-field amplitude A_{nf} and phase ϕ_{nf} by measuring the demodulated signal related to harmonics of the cantilever dynamics while varying the reference phase ϕ_{ref} in a controlled way.

> IR nanospectroscopy offers simultaneous spectroscopic access to the relationship of chemical identity and morphology with molecular-level spectroscopic specificity and spatial resolution.

For example, in two-phase homodyne detection, the reference mirror alternates between two fixed calibrated positions of $\Delta\phi_{ref} = \pi/4$. The signal at these two discrete reference phases is acquired line-by-line and allows for the calculation of images of A_{nf} and ϕ_{nf}.[15] In a recent variant termed "synthetic optical holography", a continuously varying reference phase[18] is used to reconstruct images of A_{nf} and ϕ_{nf}. Alternatively or additionally, the phase $\phi_r(\Omega_{ref})$ or amplitude $A_r(\Omega_{ref})$ can be modulated with frequency Ω_{ref}. From the resulting sidebands around the tip harmonics (Figure 2b) at $n\omega_{tip} \pm m\Omega_{ref}$, the signal $2\tilde{E}_{nf}\tilde{E}_{ref}$ can selectively be extracted.[16,17] Phase modulation, introduced to *s*-SNOM as "pseudo-heterodyne" detection, allows for real-time detection of A_{nf} and ϕ_{nf} by demodulating multiple sidebands simultaneously.[16]

Nanospectroscopy. *s*-SNOM spectra can be collected using one of the above detection schemes by collecting images of near-field $A_{nf}(\bar{\nu})$ and $\phi_{nf}(\bar{\nu})$, as shown in Figure 2c,d, across a series of wavelengths as a laser is tuned, resulting in a spectrum at each image pixel, referred to as spatiospectral imaging. With a broad-band source, a full spectrum is collected at a single point as an interferogram by scanning the reference arm. With the tip near-field interaction occurring in only one arm of the interferometer, the resulting *s*-SNOM interferograms are asymmetric (in contrast to conventional FTIR spectroscopy), as shown in Figure 2e. The Fourier transform directly yields the spectral phase and amplitude.[19,20]

Near-Field Signal Interpretation and Spectral Content. In *s*-SNOM, the scattered near-field signal is measured as a complex quantity related to the dielectric response of the tip and sample. Similar to ellipsometry, the dielectric sample response manifests as a phase delay and a change in amplitude of $\tilde{E}_{nf}$. The complex near-field, when scattered by a highly polarizable yet spectrally flat tip coupled to *local-mode* molecular sample vibrations or other intrinsic resonances $\bar{\nu}_{res}$, can be used to determine the spectral shape of the complex-valued dielectric function $\tilde{\epsilon}(\bar{\nu}) = \epsilon_1 + i\epsilon_2$ or corresponding index of refraction $\tilde{n}(\bar{\nu}) = n(\bar{\nu}) + i\kappa(\bar{\nu})$ with extinction coefficient $\kappa(\bar{\nu})$ of the sample.

The spectral *s*-SNOM phase $\phi_{nf}(\bar{\nu})$ and the $\mathrm{Im}\{\tilde{E}_{nf}(\bar{\nu})\}$ can both be used as approximate measures of $\kappa(\bar{\nu})$ for chemical identification, though spectral shifts can complicate quantitative interpretation. As an example, Figure 2f shows *s*-SNOM spectra for a typical strong molecular oscillator calculated with the spherical dipole model using experimental ellipsometry measurements of $\tilde{n}(\bar{\nu})$ for the carbonyl stretching region of bulk PMMA. The peak of $\mathrm{Im}\{\tilde{E}_{nf}(\bar{\nu})\}$ is blue-shifted by ~4 cm^{-1} relative to the peak of $\kappa(\bar{\nu})$, while $\phi_{nf}(\bar{\nu})$ is blue-shifted by ~11 cm^{-1}. However, for weaker oscillators, both $\phi_{nf}(\bar{\nu})$ and $\mathrm{Im}\{\tilde{E}_{nf}(\bar{\nu})\}$ often provide a good approximation of spectral shape and resonant frequencies of $\kappa(\bar{\nu})$.[24]

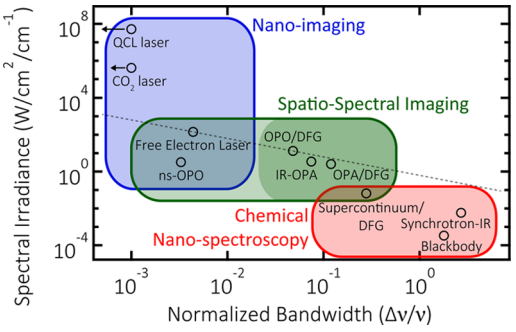

Figure 3. Summary of a selection of IR radiation sources used for IR *s*-SNOM. Spectral irradiance calculated for a 25 μm radius focal spot. Three distinct regions show sources best suited for single-wavelength nano-imaging, broad-band chemical nanospectroscopy, and spatio-spectral imaging. The gray dotted line represents a upper limit of practically usable, spectrally integrated power of ~20 mW for soft-matter *s*-SNOM.

Spectral shifts result from several contributions including the dispersive behavior of $n(\bar{\nu})$ across the resonance.[25,26] They are comparable to shifts occurring between different far-field modalities of IR spectroscopy dependent upon the angle of incidence, reflection or transmission detection, and sample geometry. *s*-SNOM spectral shifts can, in principle, be accounted for by inverting models of the tip response to obtain quantitative values for $\tilde{n}(\bar{\nu})$ or $\tilde{\epsilon}(\bar{\nu})$ of the sample.[27,28] In contrast, collective *extrinsic* resonances such as surface phonon or surface plasmon polaritons depend on the boundary conditions. Here, the near-field spectral behavior is thus more sensitive to tip geometry and tip−sample coupling, such that the spectral shape of $\tilde{\epsilon}(\bar{\nu})$ can only be determined accurately from more involved modeling of the tip−sample interaction.[29,30]

PTIR Imaging. PTIR provides for nanospectroscopy and -imaging based on molecular expansion detected as deflection of the AFM cantilever in contact mode (also termed AFM-IR).[12,31−34] On IR resonance, the pulsed laser excitation of molecular vibrations increases the effective molecular volume by thermal expansion, followed by a rapid dissipation of this excess energy over nanoscale distances. By tuning a spectrally narrow laser, an IR absorption spectrum can be obtained, with even submonolayer sensitivity when synchronizing the laser repetition rate to the cantilever dynamics.[34] However, the spatial resolution of PTIR is limited by the thermal diffusion length to about 100 nm.[32] While PTIR is well-established for linear optical nanoscale IR spectroscopy and imaging, in principle, nonlinear and coherent wave mixing spectroscopy is conceivable. However, the full range of modalities and application space of PTIR is still under-explored compared to *s*-SNOM.

Alternatively, spectroscopic imaging through mechanical cantilever sensing of the weak optical force gradient arising from the interaction of the resonantly driven molecular dipole with the tip has been proposed.[35,36] However, questions remain about assignment of the observed experimental contrast, with thermal expansion and optical force difficult to distinguish a priori.

DOI: 10.1021/acs.jpclett.5b00108
J. Phys. Chem. Lett. 2015, 6, 1275−1284

IR Sources for s-SNOM. Spectroscopic *s*-SNOM requires low noise, high spectral irradiance, and broadly tunable sources. The performance and application range of *s*-SNOM has been limited due to a lack of suitable commercially available IR light sources. A high spectral irradiance is provided by continuous-wave lasers, for example, CO, CO_2, or quantum cascade lasers (QCLs), making them suitable for nano-imaging applications, as shown in Figure 3. Their narrow tuning range allows for *s*-SNOM spectroscopy of selected vibrational modes.[8,17,25] For well-precharacterized samples, high-quality and rapid chemical nano-imaging is possible using selected marker resonances as a proxy for chemical identity and local density.

On the other hand, broad-band IR sources are highly suitable for spectroscopic *s*-SNOM.[19,20] A blackbody emitter based on a heated filament or globar provides sufficient bandwidth for collection of point spectra; though, being incoherent, it provides very low spectral irradiance.[37] A laser-based supercontinuum source offers higher spectral irradiance, allowing significant improvements in signal quality.[19] Recently, *s*-SNOM has been implemented at IR beamlines, termed synchrotron IR nanospectroscopy (SINS). Synchrotron spectral bandwidth spans the entire mid-IR from 500 to 5000 cm^{-1} with high spectral irradiance, and user facilities are making the technique increasingly available to general users.[38,39]

Maintaining necessary spectral irradiance with increasing bandwidth implies a corresponding increase in average power. However, the associated increase in both on- and off-resonant absorption leads to sample heating and damage. A solution is provided by IR sources providing high spectral irradiance over a limited bandwidth (~50−200 cm^{-1}) yet with a wide tuning range (3−20 μm).[20,40] Commercially available high repetition rate optical parametric oscillator (OPO)-based difference frequency generation (DFG) sources provide IR radiation at mW power levels with a ~100 cm^{-1} bandwidth. Alternatively, novel amplified lasers with 100s of kHz to a few MHz repetition rates and 50−100 fs pulse durations are able to pump optical parametric amplifiers (OPAs) or can be combined with a subsequent DFG process for tunable transform-limited IR generation. Additionally, the higher pulse energies of OPAs make these sources also suitable for ultrafast or nonlinear *s*-SNOM implementations. As shown in Figure 3, combined high spectral irradiance, bandwidth, and tunability may make these ideal for both imaging and spectroscopy.

Sample Selection and Limitations. As with any ultrahigh spatial resolution imaging technique, there is an associated decrease in the amount of material generating a signal for each image pixel. This imposes constraints on generating enough detectable signal for the case of weak IR modes and/or dilute sample materials.

In addition, both *s*-SNOM and PTIR rely on stable AFM operation on the sample surface. This provides constraints for imaging soft molecular surfaces, where the surface material can readily be structurally disturbed or dragged by the tip−sample force interaction. Highly porous samples or samples with large topographic variations are also not conducive for IR nano-imaging because of steric constraints of the tip apex reaching all regions.

Furthermore, despite the generally weakly perturbing nature of IR radiation, sample heating, in particular, considering additional local field enhancement by the tip, imposes a trade-off on the IR intensity between the signal level and thermal load (leading to sample softening or local melting).

Improvements to Sensitivity and Spatial Resolution. Specially engineered tips can enhance and facilitate the near-field light−matter interaction. AFM tips designed to behave as optical-frequency antennas (Figure 4) can increase the scattering cross

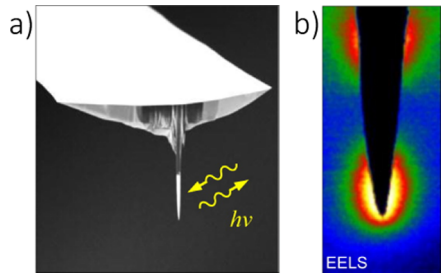

Figure 4. AFM tips with engineered dipole antenna structure shown in (a) scanning electron microscopy and (b) electron energy loss spectroscopy, reprinted from ref 42.

section of the tip, enhance local optical field strengths at the tip apex, and thus improve *s*-SNOM sensitivity. Analogous to surface-enhanced IR absorption (SEIRA) with metallic or semiconducting structures resonant in the mid-IR, with a corresponding *s*-SNOM probe, the spectral response of molecular vibrations can be enhanced.[41,42]

Spatial resolution, currently 10−20 nm, may be improved by the fabrication of sharper tips of suitable highly conductive materials at IR frequencies. Low signal levels may require spectral averaging for minutes or longer. Active stabilization of the relative lateral tip−sample position through interferometric techniques may improve spectroscopic precision and sensitivity. A combination of these and other optical and mechanical tip parameters and improved AFM stability may enable single-molecule sensitivity and spatial resolution.

Chemical Nano-Imaging Applications. We now discuss several applications that highlight the state of the art in *s*-SNOM nano-imaging and -spectroscopy performance for the investigation of soft-, biological, and small molecular matter. Spectroscopically resolved imaging allows investigation not only of chemical identity but also of vibrational signatures of a particular morphology or crystallinity on the nanoscale. With vibrational modes sensitive to inter- and intramolecular coupling, *s*-SNOM can probe local order and identify polymorphs in a range of molecular, polymeric, inorganic, or biomineral systems.

With vibrational modes sensitive to inter- and intramolecular coupling, *s*-SNOM can probe local order and identify polymorphs in a range of molecular, polymeric, inorganic, or biomineral systems.

Biomineralization often leads to crystal polymorphism, sometimes sensitively depending on environmental conditions.[43] For the prominent case of calcium carbonate, mollusk shells, for example, initially grow as calcite switching to the formation of aragonite during later life. Using broad-band *s*-SNOM, aragonite and calcite polymorph regions within the shell of a blue mussel (*Mytulis edulis*) can be distinguished by *s*-SNOM.[39,43] Figure 5a shows SINS spectra of the characteristic ν_2 and ν_3 modes of CO_3^{2-} in aragonite (880 and 1520 cm^{-1})

DOI: 10.1021/acs.jpclett.5b00108
J. Phys. Chem. Lett. 2015, 6, 1275−1284

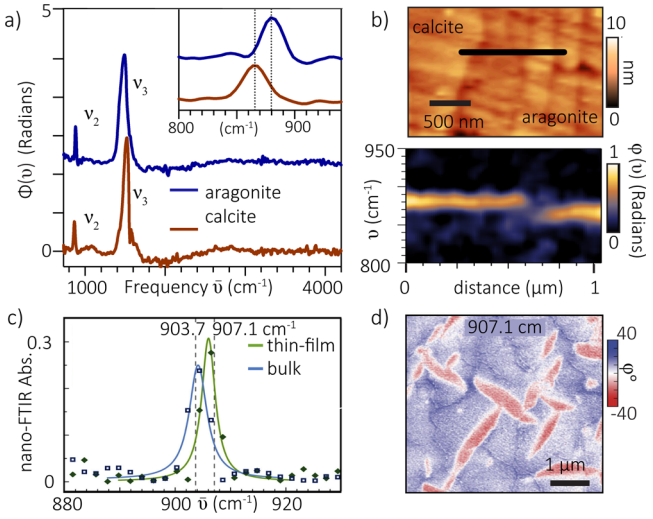

Figure 5. (a) Nanoscale spectra of carbonate polymorphs in blue mussel shell obtained with synchrotron *s*-SNOM. (b) The transition in polymorph growth from calcite to aragonite is observed in AFM height images (top) as well as in a linescan (bottom) of the spectral *s*-SNOM phase of the ν_2 mode across the transition region. (c) Thin-film and bulk-like polymorphs of pentacene are identified by a 3.4 cm^{-1} frequency difference in the hydrogen out-of-plane bending mode. (d) Corresponding near-field phase image of pentacene at 907.1 cm^{-1}, identifying the different bulk and thin-film polymorphs. (a,b) after ref 39; (c,d) reprinted from ref 44.

relative to calcite (865 and 1495 cm^{-1}). A spectrally resolved linescan of the ν_2 mode with 8 cm^{-1} spectral and 50 nm spatial resolution reveals the sharp transition between the two polymorph growth modes, in agreement with the assignment of large irregular calcite domains and smaller aragonite tiling as seen from the topography (Figure 5b).

Morphology and electronic structure are intrinsically linked in many materials, and understanding and controlling these remains an open problem in the development of organic electronic devices. Pentacene, for example, exhibits charge mobility that is highly directional and dependent on its polymorphic state. *s*-SNOM imaging of the spectral position of a hydrogen out-of-plane bending mode distinguishes bulk-phase pentacene regions based on a small but characteristic 3 cm^{-1} shift, as shown in Figure 5c.[44] *s*-SNOM phase imaging at 907.1 cm^{-1} (Figure 5d) reveals small regions of bulk-phase pentacene within a polycrystalline sample consisting primarily of thin-film phase pentacene. These results support the presence of bulk-phase pentacene crystallites, which may act as charge trap sites within thin-film phase samples.

Intermolecular Coupling and Vibrational Solvatochromism. With sufficient spatial and spectral resolution, *s*-SNOM can reach beyond identification of nanoscale domains by their chemical identity or crystallinity, toward investigation of heterogeneity in intra- and intermolecular coupling within a single chemically uniform nanoscale domain or crystallite. Vibrational resonances can shift in frequency or change in line width due to modifications in their local chemical environment. Specific marker resonances serve as sensitive probes of highly heterogeneous and coupled molecular systems, within individual nanoscale domains and at interfaces.

Using a combination of multispectral *s*-SNOM imaging with computational image analysis, the spatial inhomogeneities of intermolecular coupling can be mapped in block copolymer heterostructures, as an example.[45] Thin films of long-chain block copolymer poly(styrene-*block*-methyl methacrylate) (PMMA-*b*-PS) form kinetically frustrated and disordered quasi-lamellar structures, with significant mixing across a broad 20−40 nm wide interface. IR *s*-SNOM imaging utilizes the carbonyl resonance as a vibrational probe[19,20,25,41,46] (Figure 6a) to provide the local concentration of PMMA. Spatio-spectral imaging can then investigate local chemical environments through the spectral line shape of the carbonyl resonance at each pixel (Figure 6b).

Resulting maps of the carbonyl peak position and line width (Figure 6c,d), show shifts in the carbonyl center frequency up

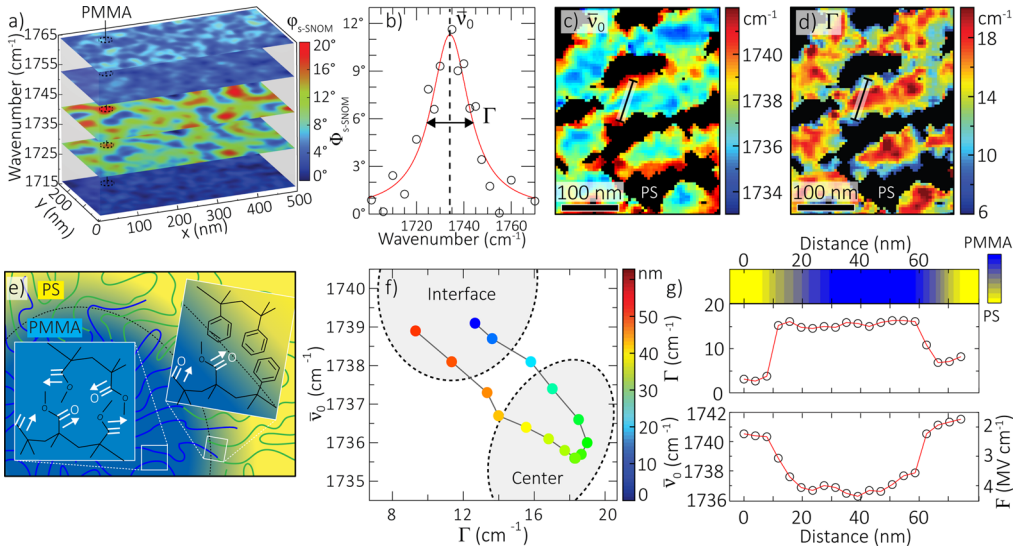

Figure 6. (a) Spatiospectral *s*-SNOM phase image of a disordered phase-separated block copolymer. (b) Point spectrum with fit to the Lorentzian line shape. (c,d) Computational line shape analysis maps of peak position $\bar{\nu}_0$ and line width Γ. (e) Schematic of PS-*b*-PMMA at the domain interface. (f) Line cut across a PMMA domain marked in (c,d), indicating the correlation between the peak shift and line width as a metric of the C═O interaction. (g) Solvation model analysis of the local spectral shift with derived variation of intermolecular field strength across domain nanointerfaces; after ref 45.

DOI: 10.1021/acs.jpclett.5b00108
J. Phys. Chem. Lett. 2015, 6, 1275−1284

to ~4 cm^{-1} and line widths varying continuously from 8 to 20 cm^{-1}. However, within this heterogeneity, the carbonyl resonance tends to be broader and red-shifted at the centers of PMMA domains compared to that at their interfaces,[45] as illustrated for a cross section through a single domain (Figure 6f). This results from underlying variation in intra- and interchain vibrational coupling, imaged through vibrational solvatochromism resulting from Stark shifts of the carbonyl mode. Figure 6g shows field strengths determined from the Stark shifts and correlation with the relative concentration of PMMA/PS. *s*-SNOM uniquely maps the local chemical environment, central to the complex interplay between the nanoscale morphology and functional properties.

Furthermore, local structure and inter- and intramolecular coupling directly affect vibrational dephasing. Dephasing dynamics change between domains of different crystallinity, domain size, and with the presence of defects. In PMMA-*b*-PS, broader peaks indicate stronger intermolecular coupling in domain centers. Variation in the line width within a single domain reveals subensemble dynamics dramatically different from the bulk behavior.

Bioimaging. The nanometer-scale organization of proteins in cell membranes is critical to their function in metabolic or signaling processes. The amide I vibrational mode is strongly IR-active, and characteristic changes in line shape can be used as a probe of secondary structure. The amide II vibration also contains information about secondary structure, and the amide III stretch has information about the relative concentration of different amino acids.

IR *s*-SNOM imaging and spectroscopy of the amide I mode has been used to study the bacteriorhodopsin (bR) protein distribution in dried purple membrane lipid bilayers.[17] As shown in Figure 7a, the $\phi_{nf}(\bar{\nu})$ signal at the center frequency of the amide I mode near 1667 cm^{-1} probes the bR density in a single membrane patch, with ~20 nm spatial resolution and a sensitivity of 2−3 protein molecules. A chemical map (b) is produced using additional correlation analysis of the topography and amide I phase (c), allowing assignment of distinct regions of mostly ordered densely packed bR, reduced bR periphery, and the largely bR depleted membrane boundary, in addition to certain defect regions of high topography yet not containing any bR.

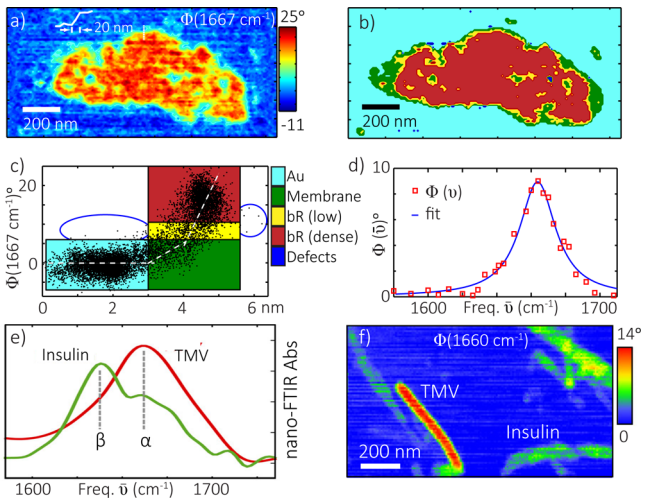

Figure 7. (a) *s*-SNOM amide I phase image of bR of a disordered dried purple membrane patch. Topography and near-field phase correlation analysis allow for the identification (b) of the Au substrate (light blue) and cell membrane (green) with flat spectral response and membrane regions of depleted (green), low (yellow), and high protein (red) concentration, as shown in (c). (d) Corresponding amide I *s*-SNOM spectrum of the dense bR region. (e) Nano-FTIR spectrum of insulin in the amide I region containing β-sheet and tobacco mosaic virus (TMV) containing α-helix structure. (f) The optical phase is used to identify aggregates of TMV and insulin. (a−d) after ref 17; (e,f) after ref 47.

Spatiospectral image analysis reveals spatially homogeneous symmetric Lorentzian line shapes (example shown in Figure 7d), indicating that the primarily α-helix character is preserved in the dried membrane. Interestingly, the characteristic amide II mode is not observed in near-field spectra.[17,47] The transition dipole moment of the amide II is perpendicular to the long axis of the α-helix and orthogonal to the transition dipole of the amide I stretch. Absence of the amide II mode indicates via selection rules that the protein has maintained an orientation within the membrane similar to that of the native protein.

In both native and engineered biological systems, several proteins may be present, or a single protein may occur in multiple folding states. Broad-band IR *s*-SNOM allows for the simultaneous nanospectroscopy of the characteristic amide mode line shapes of individual protein aggregates. Figure 7e shows IR *s*-SNOM spectra of the amide I region distinguishing a tobacco mosaic virus (TMV) with its large crystalline protein shell of primarily α-helix structure from insulin aggregates that primarily fold into β-sheet structure.[47] Corresponding fixed wavelength *s*-SNOM phase imaging tuned, for example, to the α-helix resonance at 1660 cm^{-1} (Figure 7f) allows for the label-free spatial identification of the different protein structures.

Challenges of Biological Systems. A number of challenges remain toward application of *s*-SNOM to biological systems. *s*-SNOM is an inherently surface-sensitive technique, suitable for, for example, membranes[17] or protein aggregates,[47] which to date have been demonstrated in dried samples supported on gold substrates. Topographic AFM has been demonstrated in biologically relevant buffered solutions; however, strong IR absorption by water and intermittent contact mode tip scanning both pose difficulties for *s*-SNOM implementation in liquid. Further, protein identification outside of well-defined model systems is difficult with IR spectroscopy as many proteins have similar secondary and higher-order structure.

Coherent Time-Domain Spectroscopy. An ultimate goal remains to observe local dynamics with simultaneous nanometer spatial resolution. Recently, the feasibility of femtosecond coherent vibrational dynamics[48] and incoherent pump−probe of carrier dynamics[49,50] *s*-SNOM have been demonstrated. We discuss below initial *s*-SNOM investigations of coherent vibrational dynamics and the possible extension to nonlinear multidimensional *s*-SNOM spectroscopy (Figure 8a). Coherent 2D-IR spectroscopy provides structural and dynamic information not achievable with linear spectroscopy (Figure 8b). Finally, we present implications and practical considerations for coherent control in *s*-SNOM.

With the unique subensemble probe volume smaller than that which converges in the central limit theorem and usually used to describe far-field spectroscopy, *s*-SNOM probes dynamics that promise qualitatively new physical insight beyond that achievable in traditional far-field spectroscopies. Large molecular ensembles can be described as consisting of a number of homogeneous subensembles and, when treated in the central limit theorem, give rise to a Gaussian-broadened

DOI: 10.1021/acs.jpclett.5b00108
J. Phys. Chem. Lett. 2015, 6, 1275−1284

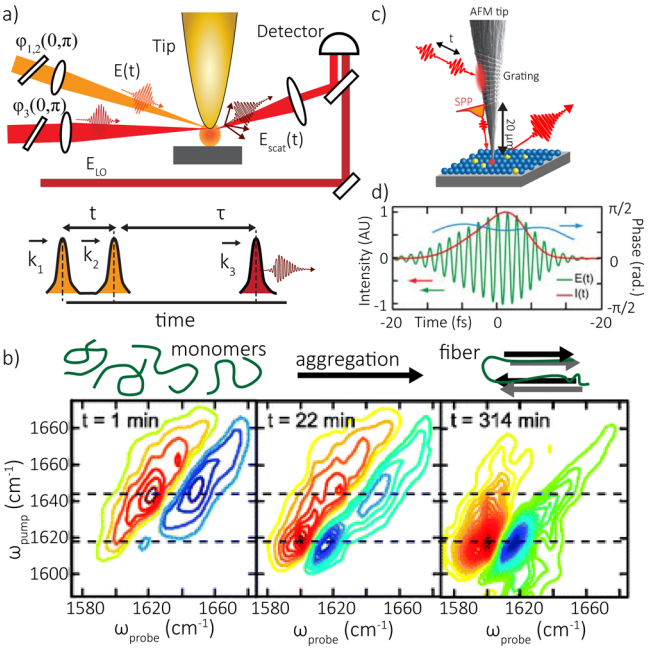

Figure 8. Considerations for ultrafast and multidimensional nonlinear *s*-SNOM: (a) Scheme for detecting the 2D-IR *s*-SNOM signal in a pump−probe or collinear geometry. Background signals are suppressed by cycling phase $\phi_i(0,\pi)$ of each pulse with wavevector $\vec{k}_i$, and the signal is optically heterodyned by the local oscillator reference field E_{LO}. (b) Far-field 2D-IR spectroscopy, as an example, tracking human islet amyloid polypeptide aggregation from a random coil into amyloid fibrils of primarily β-sheet over the course of several hours is tracked by 2D-IR spectroscopy by measuring the amide line shape to characterize the secondary structure. (c) Adiabatic focusing scheme in the near-IR. A surface plasmon polariton (SPP) launched from a grating etched on to the gold tip is focused as it propagates ∼20 μm down the conical taper of the tip. (d) The focused electric field at the tip apex reconstructed via a multiphoton intrapulse interference phase scan is compressed to 16 fs by pulse shaping. (b) after ref 55; (c) after ref 54.

optical response. A single small subensemble of only a few molecules, however, may exhibit vibrational frequencies and dephasing dynamics vastly different from the median response, even within a single-component material.

> Variation in the line width within a single domain reveals subensemble dynamics dramatically different from the bulk behavior.

Femtosecond IR *s*-SNOM has already been demonstrated in measuring the vibrational free-induction decay of a small subensemble within the 20 nm probe volume of the *s*-SNOM tip. Probing the vibrational free-induction decay of C−F stretch vibrations in polytetrafluoroethylene (PTFE), additional scatterers created by the deposition of gold particles contribute to dephasing through radiative or nonradiative decay channels.[48] Similar subensemble investigations have been performed with coherent time domain anti-Stokes Raman spectroscopy in a nanoparticle pair geometry.[51] These experiments, together with other tip-scattering second- and third-order experiments, indicate the possible extension of *s*-SNOM to nonlinear coherent ultrafast spectroscopy.[52−54]

Two-dimensional spectroscopy enables the investigation of coupling between vibrational[56] or electronic[57] states through the appearance of cross peaks, as well as distinguishing competing pathways in ground- or excited-state motion.[58,59] In the IR, time-dependent cross peaks provide information on vibrational coupling, energy flow, and molecular structure. Inhomogeneous broadening can be separated along the diagonal from homogeneous dephasing times. Figure 8b illustrates additional structural information that can be measured with 2D-IR, based on changes in line shape to monitor, for example, β-sheet formation from an initially random coil protein. In many cases, it is difficult to determine spatial correlation between spectral features, such as whether the random coil and β-sheet can be found in a partially folded fibril during intermediate times. Nanoscale spatial and morphological information could make 2D-IR *s*-SNOM a natural extension toward investigating structural correlation and heterogeneity in vibrational coupling.

Conventional multidimensional and other nonlinear optical spectroscopies rely on phase matching of incident and detected beams as increasing numbers of interaction pathways contribute to observable signals. A number of methods for separating specific Feynman pathways have been developed, which rely on carefully designed optical interaction geometries with spatial selection of specific wave vectors of the phase-matched third-order interactions of interest. However, as with any nonlinear light scattering process in the Rayleigh limit,[60] due to the lack of macroscopic translational invariance, phase matching and spatial wave vector selection is not possible in nanostructured materials. Scattering by sample inhomogeneity or even the sample window leads to the spatial superposition and interference of different nonlinear interaction terms (Figure 8a), which introduces artifacts even in far-field multidimensional spectroscopy.[61] For the same fundamental reason, due to the scattering nature of the *s*-SNOM tip, it is not possible to separate the weak third-order signal from dominant linear and incoherent pump−probe contributions at the same frequency through geometric arrangement of incident and detected beams.

To a limited extent, polarization control schemes have been used in far-field spectroscopy,[62] but poorly controlled and anisotropic scattering of the induced tip polarization makes schemes based upon polarization control particularly difficult to use in *s*-SNOM. Methods using phase cycling or quasi-phase cycling of the optical pulses have recently been developed to suppress unwanted signals in far-field 2D-IR spectroscopy of highly scattering samples.[61] Because the 2D signal depends on the phases of each of the three incident pulses, $\phi_{2D-IR} = \pm\phi_1 \mp \phi_2 + \phi_3$, the 2D signal can be selectively detected by cycling the phase of each pulse. Phase cycling methods have enabled 2D-IR investigations of amides adsorbed to Au nanoparticles.[63] More recently, 2D-IR based in a fully collinear geometry has been demonstrated for diffraction-limited far-field vibrational lifetime imaging using a combination of polarization selection, phase cycling, and amplitude modulation.[64] Phase cycling is thus expected to be an enabling requirement for future development of 2D-IR *s*-SNOM spectroscopy. One possible detection scheme is shown in Figure 8a, allowing for the detection of relevant rephasing, nonrephasing, or purely absorptive pathways following established phase cycling procedures.[55]

s-SNOM spectroscopy is fundamentally compatible with any type of higher-order spectroscopy as tip scattering is a low-dispersion process and each field interaction can be described

DOI: 10.1021/acs.jpclett.5b00108
J. Phys. Chem. Lett. 2015, 6, 1275−1284

by its higher-order optical susceptibility. Higher-order optical processes are possible at the tip apex even at the relatively low average powers and high repetition rates necessary for *s*-SNOM as a result of electric field enhancements of $\geq$10.[60] Engineered tips may further enhance electric field strengths from ultrashort laser pulses. One approach, optical nanofocusing on a tip through adiabatic transformation of a surface plasmon polariton coupled to a conical taper (Figure 8c), enables background suppression, femtosecond control through laser pulse shaping, quantum coupling, and impedance matching to quantum systems.[54] With active-phase control through pulse shaping, a nearly transform-limited 16 fs pulse is measured from the tip apex, with the reconstructed phase shown in Figure 8d. Although this approach can not readily be extended to the mid-IR, it demonstrates the concept of optical coherence on the tip, and similar concepts can be used in implementation of third-order IR spectroscopy.

In conclusion, *s*-SNOM localizes coherent femtosecond optical excitation on a polarizable conducting tip, inducing vibrational or electronic excitation with high coupling efficiency. Vibrational spectroscopy with nanometer resolution enables the investigation of chemical composition with sensitivity to polymorph identity, crystallinity, molecular orientation, domain orientation, domain interfaces, and coupling between molecules or between neighboring domains. Augmented by new source developments, pulse shaping, and tips with engineered optical response, it is possible to extend ultrafast electronic and vibrational spectroscopy to the nanoscale, with progress already reaching single-protein sensitivity and ultimately that of a single local oscillator. Through generalization of the near-field light–matter interaction, it becomes possible to obtain femtosecond time domain spectroscopy with nanometer spatial resolution in order to probe the relationship between nanoscale morphology and material function.

AUTHOR INFORMATION

Corresponding Author

*E-mail: markus.raschke@colorado.edu.

Notes

The authors declare no competing financial interest.

Biographies

Eric A. Muller is a Postdoc at the University of Colorado at Boulder. His research includes developing applications of synchrotron infrared near-field spectroscopy, nanoscale control of light–matter interaction, and single-molecule dynamics. He received his Ph.D. from the University of California Berkeley in 2012.

Benjamin Pollard is a physics Ph.D. student at the University of Colorado at Boulder. His research focuses on multimodal chemical nano-imaging of soft-matter and the development of related mid-IR femtosecond laser sources. He received his bachelor's degree from Pomona College in 2011.

Markus B. Raschke is Professor at the University of Colorado at Boulder. His group develops nanospectroscopic imaging techniques to study soft-matter and correlated electron materials and to probe their nonlinear and ultrafast quantum dynamics. He received his Ph.D. in 2000 from the Max-Planck-Institute for Quantum Optics in Munich.

ACKNOWLEDGMENTS

The authors thank Joanna Atkin, Hans Bechtel, Omar Khatib, Mike Martin, Scott Lea, and Tom Perkins for stimulating collaborations and discussions. M.B.R acknowledges support through a partner proposal with the Environmental Molecular Sciences Laboratory (EMSL), a national scientific user facility from the DOE Office of Biological and Environmental Research at Pacific Northwest National Laboratory (PNNL). PNNL is operated by Battelle for the U.S. DOE under Contract DEAC06-76RL01830. E.A.M. and M.B.R. thank the Advanced Light Source for support, which is supported by the Director, Office of Science, Office of Basic Energy Sciences, of the U.S. Department of Energy under Contract No. DE-AC02-05CH11231. Funding from the National Science Foundation (NSF Grant CHE 1306398) is gratefully acknowledged.

REFERENCES

(1) Ade, H.; Stoll, H. Near-Edge X-ray Absorption Fine-Structure Microscopy of Organic and Magnetic Materials. *Nat. Mater.* **2009**, *8*, 281–290.

(2) Hitchcock, A. P.; Dynes, J. J.; Johansson, G.; Wang, J.; Botton, G. Comparison of NEXAFS Microscopy and TEM-EELS for Studies of Soft Matter. *Micron* **2008**, *39*, 311–319.

(3) Hell, S. W. Far-Field Optical Nanoscopy. *Science* **2007**, *316*, 1153–1158.

(4) Betzig, E.; Patterson, G. H.; Sougrat, R.; Lindwasser, O. W.; Olenych, S.; Bonifacino, J. S.; Davidson, M. W.; Lippincott-Schwartz, J.; Hess, H. F. Imaging Intracellular Fluorescent Proteins at Nanometer Resolution. *Science* **2006**, *313*, 1642–1645.

(5) Pohl, D. W.; Denk, W.; Lanz, M. Optical Stethoscopy: Image Recording with Resolution λ/20. *Appl. Phys. Lett.* **1984**, *44*, 651.

(6) Betzig, E.; Trautman, J. K.; Harris, T. D.; Weiner, J. S. Breaking the Diffraction Barrier: Optical Microscopy. *Science* **1991**, *251*, 1468–1470.

(7) Knoll, B.; Keilmann, F. Near-Field Probing of Vibrational Aborption for Chemical Microscopy. *Nature* **1999**, *399*, 134–137.

(8) Brehm, M.; Taubner, T.; Hillenbrand, R.; Keilmann, F. Infrared Spectroscopic Mapping of Single Nanoparticles and Viruses at Nanoscale Resolution. *Nano Lett.* **2006**, *6*, 1307–1310.

(9) Wessel, J. Surface-Enhanced Optical Microscopy. *J. Opt. Soc. Am. B* **1985**, *2*, 1538–1541.

(10) Inouye, Y.; Kawata, S. Near-Field Scanning Optical Microscope with a Metallic Probe Tip. *Opt. Lett.* **1994**, *19*, 159.

(11) Zenhausern, F.; Martin, Y.; Wickramasinghe, H. K. Scanning Interferometric Apertureless Microscopy: Optical Imaging at 10 Angstrom Resolution. *Science* **1995**, *269*, 1083–1085.

(12) Dazzi, A.; Prazeres, R.; Glotin, F.; Ortega, J. M. Local Infrared Microspectroscopy with Subwavelength Spatial Resolution with an Atomic Force Microscope Tip Used as a Photothermal Sensor. *Opt. Lett.* **2005**, *30*, 2388.

(13) Keilmann, F., Hillenbrand, R. In *Nano-optics and Near-Field Optical Microscopy*; Zayats, A., Richards, D., Eds.; Artech House, Inc.: Norwood, MA, 2009; Chapter 11, pp 235–266.

(14) Atkin, J. M.; Berweger, S.; Jones, A. C.; Raschke, M. B. Nano-Optical Imaging and Spectroscopy of Order, Phases, and Domains in Complex Slids. *Adv. Phys.* **2012**, *61*, 745–842.

(15) Taubner, T.; Hillenbrand, R.; Keilmann, F. Performance of Visible and Mid-Infrared Scattering-Type Near-Field Optical Microscopes. *J. Microsc.* **2003**, *210*, 311–314.

(16) Ocelic, N.; Huber, A.; Hillenbrand, R. Pseudoheterodyne Detection for Background-Free Near-Field Spectroscopy. *Appl. Phys. Lett.* **2006**, *89*, 101124.

(17) Berweger, S.; Nguyen, D. M.; Muller, E. A.; Bechtel, H. A.; Perkins, T. T.; Raschke, M. B. Nano-chemical Infrared Imaging of Membrane Proteins in Lipid Bilayers. *J. Am. Chem. Soc.* **2013**, *135*, 18292–18295.

(18) Schnell, M.; Carney, P. S.; Hillenbrand, R. Synthetic Optical Holography for Rapid Nanoimaging. *Nat. Commun.* **2014**, *5*, 3499.

(19) Huth, F.; Govyadinov, A.; Amarie, S.; Nuansing, W.; Keilmann, F.; Hillenbrand, R. Nano-FTIR Absorption Spectroscopy of Molecular

DOI: 10.1021/acs.jpclett.5b00108
J. Phys. Chem. Lett. 2015, 6, 1275–1284

Fingerprints at 20 nm Spatial Resolution. *Nano Lett.* **2012**, *12*, 3973−3978.
(20) Xu, X. G.; Rang, M.; Craig, I. M.; Raschke, M. B. Pushing the Sample-Size Limit of Infrared Vibrational Nanospectroscopy: From Monolayer toward Single Molecule Sensitivity. *J. Phys. Chem. Lett.* **2012**, *3*, 1836−1841.
(21) Raschke, M. B.; Lienau, C. Apertureless Near-Field Optical Microscopy: Tip-Sample Coupling in Elastic Light Scattering. *Appl. Phys. Lett.* **2003**, *83*, 5089.
(22) Akhremitchev, B. B.; Pollack, S.; Walker, G. C. Apertureless Scanning Near-Field Infrared Microscopy of a Rough Polymeric Surface. *Langmuir* **2001**, *17*, 2774−2781.
(23) Gomez, L.; Bachelot, R.; Bouhelier, A.; Wiederrecht, G. P.; Chang, S.; Gray, S. K.; Hua, F.; Jeon, S.; Rogers, J. A.; Castro, M. E.; Blaize, S.; Stefanon, I.; Lerondel, G.; Royer, P. Apertureless Scanning Near-Field Optical Microscopy: A Comparison Between Homodyne and Heterodyne Approaches. *J. Opt. Soc. Am. B* **2006**, *23*, 823−833.
(24) The model assumptions in Xu et al. 2012[20] based on ϵ_1 being only weakly frequency-dependent on resonance, only provide a good approximation of the spectral *s*-SNOM phase to describe the absorption spectrum of a material for weak vibrational oscillators.
(25) Taubner, T.; Hillenbrand, R.; Keilmann, F. Nanoscale Polymer Recognition by Spectral Signature in Scattering Infrared Near-Field Microscopy. *Appl. Phys. Lett.* **2004**, *85*, 5064.
(26) Mastel, S.; Govyadinov, A. A.; de Oliveira, T. V. A. G.; Amenabar, I.; Hillenbrand, R. Nanoscale-Resolved Chemical Identification of Thin Organic Films Using Infrared Near-Field Spectroscopy and Standard Fourier Transform Infrared References. *Appl. Phys. Lett.* **2015**, *106*, 023113.
(27) Hauer, B.; Engelhardt, A. P.; Taubner, T. Quasi-Analytical Model for Scattering Infrared Near-Field Microscopy on Layered Systems. *Opt. Express* **2012**, *20*, 13173−13188.
(28) Govyadinov, A. A.; Amenabar, I.; Huth, F.; Carney, P. S.; Hillenbrand, R. Quantitative Measurement of Local Infrared Absorption and Dielectric Function with Tip-Enhanced Near-Field Microscopy. *J. Phys. Chem. Lett.* **2013**, *4*, 1526−1531.
(29) Cvitkovic, A.; Ocelic, N.; Hillenbrand, R. Analytical Model for Quantitative Prediction of Material Contrasts in Scattering-Type Near-Field Optical Microscopy. *Opt. Express* **2007**, *15*, 8550.
(30) McLeod, A. S.; Kelly, P.; Goldflam, M. D.; Gainsforth, Z.; Westphal, A. J.; Dominguez, G.; Thiemens, M. H.; Fogler, M. M.; Basov, D. N. Model for Quantitative Tip-Enhanced Spectroscopy and the Extraction of Nanoscale-Resolved Optical Constants. *Phys. Rev. B* **2014**, *90*, 085136.
(31) Kjoller, K.; Felts, J. R.; Cook, D.; Prater, C. B.; King, W. P. High-Sensitivity Nanometer-Scale Infrared Spectroscopy Using a Contact Mode Microcantilever with an Internal Resonator Paddle. *Nanotechnology* **2010**, *21*, 185705.
(32) Marcott, C.; Lo, M.; Kjoller, K.; Prater, C.; Noda, I. Spatial Differentiation of Sub-Micrometer Domains in a Poly-(hydroxyalkanoate) Copolymer Using Instrumentation that Combines Atomic Force Microscopy (AFM) and Infrared (IR) Spectroscopy. *Appl. Spectrosc.* **2011**, *65*, 1145−1150.
(33) Katzenmeyer, A. M.; Aksyuk, V.; Centrone, A. Nanoscale Infrared Spectroscopy: Improving the Spectral Range of the Photothermal Induced Resonance Technique. *Anal. Chem.* **2013**, *85*, 1972−1979.
(34) Lu, F.; Jin, M.; Belkin, M. A. Tip-Enhanced Infrared Nanospectroscopy via Molecular Expansion Force Detection. *Nat. Photonics* **2014**, *8*, 307−312.
(35) Rajapaksa, I.; Uenal, K.; Wickramasinghe, H. K. Image Force Microscopy of Molecular Resonance: A Microscope Principle. *Appl. Phys. Lett.* **2010**, *97*, 7−10.
(36) Kohlgraf-Owens, D. C.; Sukhov, S.; Greusard, L.; de Wilde, Y.; Dogariu, A. Optically Induced Forces in Scanning Probe Microscopy. *Nanophotonics* **2014**, *3*, 105−116.
(37) Huth, F.; Schnell, M.; Wittborn, J.; Ocelic, N.; Hillenbrand, R. Infrared-Spectroscopic Nanoimaging with a Thermal Source. *Nat. Mater.* **2011**, *10*, 352−356.
(38) Hermann, P.; Hoehl, A.; Ulrich, G.; Fleischmann, C.; Hermelink, A.; Kästner, B.; Patoka, P.; Hornemann, A.; Beckhoff, B.; Rühl, E.; et al. Characterization of Semiconductor Materials Using Synchrotron Radiation-Based Near-Field Infrared Microscopy and Nano-FTIR Spectroscopy. *Opt. Express* **2014**, *22*, 17948−17958.
(39) Bechtel, H. A.; Muller, E. A.; Olmon, R. L.; Martin, M. C.; Raschke, M. B. Ultrabroadband Infrared Nanospectroscopic Imaging. *Proc. Natl. Acad. Sci. U.S.A.* **2014**, *111*, 7191−7196.
(40) Bensmann, S.; Gaußmann, F.; Lewin, M.; Wüppen, J.; Nyga, S.; Janzen, C.; Jungbluth, B.; Taubner, T. Near-Field Imaging and Spectroscopy of Locally Strained GaN Using an IR Broadband Laser. *Opt. Express* **2014**, *22*, 22369−22381.
(41) Hoffman, J. M.; Hauer, B.; Taubner, T. Antenna-Enhanced Infrared Near-Field Nanospectroscopy of a Polymer. *Appl. Phys. Lett.* **2012**, *101*, 193105.
(42) Huth, F.; Chuvilin, A.; Schnell, M.; Amenabar, I.; Krutokhvostov, R.; Lopatin, S.; Hillenbrand, R. Resonant Antenna Probes for Tip-Enhanced Infrared Near-Field Microscopy. *Nano Lett.* **2013**, *13*, 1065−1072.
(43) Amarie, S.; Zaslansky, P.; Kajihara, Y.; Griesshaber, E.; Schmahl, W. W.; Keilmann, F. Nano-FTIR Chemical Mapping of Minerals in Biological Materials. *Beilstein J. Nanotechnol.* **2012**, *3*, 312−323.
(44) Westermeier, C.; Cernescu, A.; Amarie, S.; Liewald, C.; Keilmann, F.; Nickel, B. Sub-Micron Phase Coexistence in Small-Molecule Organic Thin Films Revealed by Infrared Nano-Imaging. *Nat. Commun.* **2014**, *5*, 4101.
(45) Pollard, B.; Muller, E. A.; Hinrichs, K.; Raschke, M. B. Vibrational Nano-Spectroscopic Imaging Correlating Structure with Intermolecular Coupling and Dynamics. *Nat. Commun.* **2014**, *5*, 3587.
(46) Filimon, M.; Kopf, I.; Schmidt, D. A.; Brundermann, E.; Ruhe, J.; Santer, S.; Havenith, M. Local Chemical Composition of Nanophase-Separated Polymer Brushes. *Phys. Chem. Chem. Phys.* **2011**, *13*, 11620−11626.
(47) Amenabar, I.; Poly, S.; Nuansing, W.; Hubrich, E. H.; Govyadinov, A. A.; Huth, F.; Krutokhvostov, R.; Zhang, L.; Knez, M.; Heberle, J.; et al. Structural Analysis and Mapping of Individual Protein Complexes by Infrared Nanospectroscopy. *Nat. Commun.* **2013**, *4*, 2890.
(48) Xu, X. G.; Raschke, M. B. Near-Field Infrared Vibrational Dynamics and Tip-Enhanced Decoherence. *Nano Lett.* **2013**, *13*, 1588−1595.
(49) Wagner, M.; McLeod, A. S.; Maddox, S. J.; Fei, Z.; Liu, M.; Averitt, R. D.; Fogler, M. M.; Bank, S. R.; Keilmann, F.; Basov, D. N. Ultrafast Dynamics of Surface Plasmons in InAs by Time-Resolved Infrared Nanospectroscopy. *Nano Lett.* **2014**, *14*, 4529−4534.
(50) Eisele, M.; Cocker, T. L.; Huber, M. A.; Plankl, M.; Viti, L.; Ercolani, D.; Sorba, L.; Vitiello, M. S.; Huber, R. Ultrafast Multi-Terahertz Nano-Spectroscopy with Sub-Cycle Temporal Resolution. *Nat. Photonics* **2014**, *8*, 841−845.
(51) Yampolsky, S.; Fishman, D.; Dey, S.; Hulkko, E.; Banik, M.; Potma, E.; Apkarian, V. Seeing a Single Molecule Vibrate through Time-Resolved Coherent Anti-Stokes Raman Scattering. *Nat. Photonics* **2014**, *8*, 650−656.
(52) Ichimura, T.; Hayazawa, N.; Hashimoto, M.; Inouye, Y.; Kawata, S. Tip-Enhanced Coherent Anti-Stokes Raman Scattering for Vibrational Nanoimaging. *Phys. Rev. Lett.* **2004**, *92*, 220801.
(53) Danckwerts, M.; Novotny, L. Optical Frequency Mixing at Coupled Gold Nanoparticles. *Phys. Rev. Lett.* **2007**, *98*, 026104.
(54) Berweger, S.; Atkin, J. M.; Xu, X. G.; Olmon, R. L.; Raschke, M. B. Femtosecond Nanofocusing with Full Optical Waveform Control. *Nano Lett.* **2011**, *11*, 4309−4313.
(55) Shim, S.-H.; Zanni, M. T. How to Turn Your Pump−Probe Instrument into a Multidimensional Spectrometer: 2D IR and Vis Spectroscopies Via Pulse Shaping. *Phys. Chem. Chem. Phys.* **2009**, *11*, 748−761.
(56) Pakoulev, A. V.; Rickard, M. A.; Mathew, N. A.; Kornau, K. M.; Wright, J. C. Frequency-Domain Time-Resolved Four Wave Mixing Spectroscopy of Vibrational Coherence Transfer with Single-Color Excitation. *J. Phys. Chem. A* **2008**, *112*, 6320−6329.

DOI: 10.1021/acs.jpclett.5b00108
J. Phys. Chem. Lett. 2015, 6, 1275−1284

(57) Moody, G.; Akimov, A. I.; Li, H.; Singh, R.; Yakovlev, R. D.; Karczewski, G.; Wiater, M.; Wojtowicz, T.; Bayer, M.; Cundiff, T. S. Coherent Coupling of Excitons and Trions in a Photoexcited CdTe/CdMgTe Quantum Well. *Phys. Rev. Lett.* **2014**, *112*, 097401.
(58) Lai, Z.; Preketes, N.; Mukamel, S.; Wang, J. Monitoring the Folding of Trp-Cage Peptide by Two-Dimensional Infrared (2DIR) Spectroscopy. *J. Phys. Chem. B* **2013**, *117*, 4661−4669.
(59) Calhoun, T. R.; Davis, J. A.; Graham, M. W.; Fleming, G. R. The Separation of Overlapping Transitions in β-Carotene with Broadband 2D Electronic Spectroscopy. *Chem. Phys. Lett.* **2012**, *523*, 1−5.
(60) Neacsu, C. C.; Reider, G. A.; Raschke, M. B. Second-Harmonic Generation from Nanoscopic Metal Tips: Symmetry Selection Rules for Single Asymmetric Nanostructures. *Phys. Rev. B* **2005**, *71*, 201402.
(61) Bloem, R.; Garrett-Roe, S.; Strzalka, H.; Hamm, P.; Donaldson, P. Enhancing Signal Detection and Completely Eliminating Scattering Using Quasi-Phase-Cycling in 2D IR Experiments. *Opt. Express* **2010**, *18*, 27067−27078.
(62) Zanni, M. T.; Ge, N.-H.; Kim, Y. S.; Hochstrasser, R. M. Two-Dimensional IR Spectroscopy Can be Designed to Eliminate the Diagonal Peaks and Expose Only the Crosspeaks Needed for Structure Determination. *Proc. Natl. Acad. Sci. U.S.A.* **2001**, *98*, 11265−11270.
(63) Donaldson, P. M.; Hamm, P. Gold Nanoparticle Capping Layers: Structure, Dynamics, and Surface Enhancement Measured Using 2D-IR Spectroscopy. *Angew. Chem., Int. Ed.* **2013**, *52*, 634−638.
(64) Baiz, C. R.; Schach, D.; Tokmakoff, A. Ultrafast 2D IR Microscopy. *Opt. Express* **2014**, *22*, 18724−18735.

DOI: 10.1021/acs.jpclett.5b00108
J. Phys. Chem. Lett. 2015, 6, 1275−1284